Analysis of Heat and Mass Transfer on Free Moving Urea/Water-Droplets in SCR-Systems by Numerical Methods

Lukas Möltner, Aldo Giovannini, and Verena Schallhart

***Abstract*—**The selective catalytic reduction (SCR) of nitrogen oxides (NO_x) is the most promising technique to meet prospective emission regulations. Due to its toxic potential the reducing agent ammonia cannot be stored in a car, but it can be carried in the form of an urea-water-solution (UWS), which is injected into the hot exhaust gas and reacts to ammonia. This generation of ammonia upstream the catalytic converter is responsible for the efficiency of the complete SCR-process-chain. This study deals with the analysis and description of interactions between droplets of urea-water-solution and the exhaust gas. For the description of the droplets´ trajectories a numeric model was developed, which considers contrary to previous surveys the loss of the droplets´ mass due to evaporation of water and thermal decomposition of urea. The model for the droplets´ motion includes an evaporation model for binary fluids and it was extended by a kinetic approach to describe the thermal decomposition. This model is able to determine the exact position of the flying droplet, velocity, composition, current temperature and thermo- and fluid-dynamic parameters. These parameters are substantial for the discussion of the heat and mass transfer between droplets and exhaust gas.

***Keywords*—**AdBlue®, Diesel engines, Exhaust gas after-treatment, NO_x, SCR

I. Introduction

DIESEL engines present in combination with turbochargers and modern fuel injection systems constant high torque over a wide speed range and therefore excellent driving performance. These characteristics are the reason for its popularity. At present, almost 50% of all passenger vehicles in Europe are diesel-driven [1]. A major challenge in the future is to meet increasingly stringent emission regulations without dramatically rising costs of power train units [2]. Particularly the strictly limited nitrogen oxides and particulate matter (PM) emissions require great efforts, Fig. 1.

The most promising technology to reduce nitrogen oxides (NO_x) emissions in passenger cars and commercial vehicles is the selective catalytic reduction with ammonia. Due to the fact that a separate reducing agent tank is required to use selective catalytic reduction (SCR) technology in cars and possible leaks in the tank and piping system can be classified as very harmful because of the toxicity of ammonia, only SCR systems with NH_3-releasing substances are available or developed. These substances, e.g. urea, feature a clearly smaller toxicity and can be stored and dosed as an aqueous solution. At present, a distribution network, for the standardized urea-water-solution according to DIN 70700, is established. UWS contains 32.5wt.-% urea and is sold under the brand name AdBlue®.

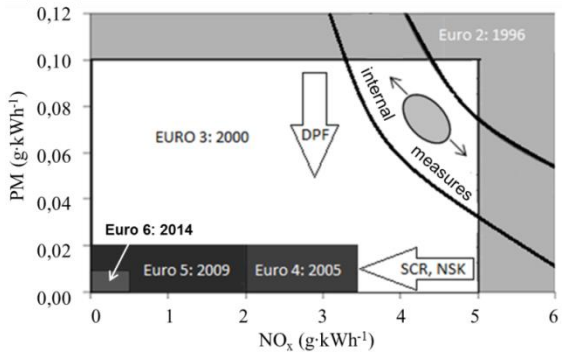

Fig. 1: Progress of emission restrictions in Europe [3]

The determining factor for a moderate reducing agent consumption and the efficiency of SCR systems is the sufficient ammonia generation and homogenization upstream the catalytic converter.

Subsequently to the evaporation of water out of the UWS droplets and the melting of urea, the formation of ammonia occurs in two single reactions. In the first reaction (1), a thermolytic decomposition of urea to ammonia and isocyanic acid takes place. Another mole of ammonia and CO_2 are produced from the isocyanic acid by hydrolysis, (2).

$$(NH_2)2CO \leftrightarrow NH_3 + HNCO \quad (1)$$

$$HNCO + H_2O \leftrightarrow NH_3 + CO_2 \quad (2)$$

The mixing section between the UWS-injection and the entrance in the catalytic converter is shown in the process chain below, Fig. 2. Furthermore, Fig. 2 shows the direction of the UWS-injection for both investigated cases, on the one hand the coflow-injection ❶ and on the other hand the counterflow-injection ②.

Lukas Möltner is with the Department of Technology and Life Sciences, Management Center Innsbruck - Austria (phone: + 43 512 2070 – 3835; e-mail: lukas.moeltner@mci.edu).

Aldo Giovannini is with the Department of Technology and Life Sciences, Management Center Innsbruck - Austria (e-mail: aldo.giovannini@mci.edu).

Verena Schallhart is with the Department of Technology and Life Sciences, Management Center Innsbruck - Austria (e-mail: verena.schallhart@mci.edu).

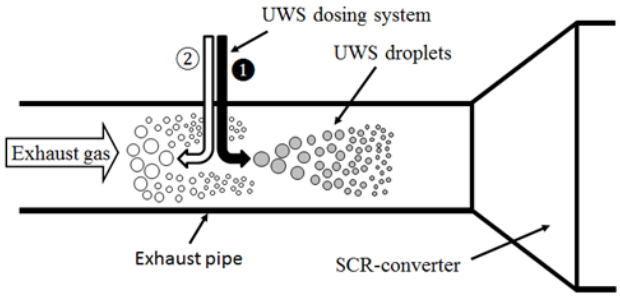

Fig. 2: Insertion of UWS into the mixing section of an SCR-system with coflow-injection ❶ and counterflow-injection ②

The objective of this study is to analyze the heat and mass transfer on UWS-droplets during the flight phase between insertion and entrance in the catalytic converter. In detail, the direction of injection will be observed by numerical simulation under accurate consideration of occurring droplet/gas-interactions. Especially the influence of a counterflow injection to the droplet evaporation is investigated.

The results of these investigations will provide a basis for the development of highly effective mixing sections for future SCR-systems.

II. Fundamentals

The description of droplets´ motion in a surrounding gas flow is based on the balance of forces acting on a droplet, Fig. 3.

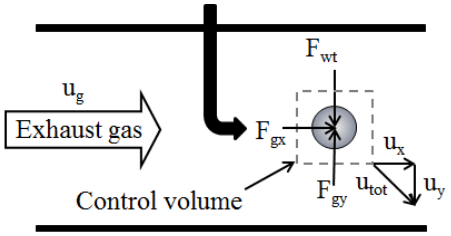

Fig. 3: Balance of forces on a moving droplet

This balance provides the basis for the equation of motion and further for the multi-dimensional motion model, which considers each spatial-axis and thus determines the droplet velocity and the droplet position. The starting point is the droplet movement with an initial velocity and directed motion.

In total, the sum of the single gas forces F_g and the weight F_{wt} are acting on a moving droplet and cause a change in its velocity $d\vec{u}_{dr}/dt$, (3), according to Newton's principle of action.

$$m_{dr}\frac{d\vec{u}_{dr}}{dt} = \vec{F}_g + \vec{F}_{wt} \tag{3}$$

The gas force F_g is the product of the projected area A_{pr}, the drag coefficient for drops c_{dr} and the dynamic pressure, (4).

$$\vec{F}_g = A_{pr} * c_{dr}\frac{\rho_g * |\vec{u}_{rel}| * \vec{u}_{rel}}{2} \tag{4}$$

The calculation of the drag coefficient requires the calculation of the Reynolds number, which is determined by the droplet diameter D_{dr}, the exhaust gas density ρ_g and the dynamic viscosity u_g, (5).

$$Re_{dr} = \frac{\rho_g * |\vec{u}_{rel}| * D_{dr}}{\mu_g} \tag{5}$$

The drag coefficient for droplets with a Reynolds number $Re_{dr} < 800$ is calculated by (6).

$$c_{dr} = \frac{24}{Re_{dr}}(1 + 0{,}15 * {Re_{dr}}^{0{,}687}) \tag{6}$$

For Reynolds numbers $Re_{dr} > 800$, (7) comes into effect [4].

$$c_{Tr} = 0{,}44 \tag{7}$$

The acting force caused by gravity and buoyancy is calculated by the droplet volume V_{dr}, the droplet density ρ_{dr} and the gas density ρ_g. Insertions and transformations lead to (8), which describes after integration the droplets velocity.

$$\frac{d\vec{u}_{dr}}{dt} = \frac{3}{4} * \frac{\mu_g * c_{dr} * Re_{dr}}{\rho_{Tr} * {D_{dr}}^2} * * \left(\vec{u}_g - d\right) + \left(1 - \frac{\rho_g}{\rho_{dr}}\right) * \vec{g} \tag{8}$$

The motion vector is the result of reintegration, (9):

$$\frac{d\vec{x}_{dr}}{dt} = \vec{u}_{dr} \tag{9}$$

This equation is the basis for the presented simulation model and is state of the art for describing droplets' motion, e.g. [4]. However, this model only considers droplets with constant weight as well as constant material characteristics and temperature without observing changes caused by evaporation or chemical reactions.

The next chapter presents the implementation of an evaporation model and a kinetic approach to extend the capabilities of the model.

III. Methodology

A. Modeling the droplet evaporation

In case of a change in weight and size due to evaporation and/or thermal decomposition the capabilities of the model have to be extended by these two sub-processes.

For the simulation of sprays a Lagrangian approach was chosen. In this approach the calculation of droplets' trajectories and heat and mass transfer is only considered for a statistically representative number of droplets inside a magnitude instead of the whole droplet collective.

Nusselt describes the evaporation as a diffusion phenomenon in a thin interphase between the droplet and the surrounding gas, subjected to the condition that the relative humidity of the surrounding gas is $X_g<1$. Furthermore, the evaporation occurs faster if the droplet is continuously circulated by gas compared to a static gaseous atmosphere. Equation (10) describes the mass transfer coefficient k_M, which is determined by the dimensionless Sherwood number Sh and the diffusion coefficient D [5].

$$Sh_{(t)} \equiv \frac{k_M * D_{dr(t)}}{D} = \\ = 2 + 0{,}6 * Re_{dr(t)}{}^{\frac{1}{2}} * Sc^{\frac{1}{3}} \quad (10)$$

The Schmidt number Sc is delivered by (11).

$$Sc = \frac{\mu_g}{\rho_g * D} \quad (11)$$

The diffusion coefficient D of vapour into air is determined by current and reference temperature and pressure, (12).

$$D_{(T,p)} = 22{,}2 * 10^{-6} * \left(\frac{T}{T_0}\right) * \frac{p_0}{p} \quad (12)$$

These equations were approved by experiments with drops of different liquids and diameter classes by Ranz and Marshall in [6]. Subsequently the weight loss rate of droplets due to evaporation can be calculated by (13). The diffusion of vapor in exhaust gas occurs on the droplets' surface A_{sf}. It is quantitatively influenced by the mass transfer coefficient k_M and by the driving force for diffusion phenomena, the vapour pressure $p_{v(Tg)}$. M_{H2O} represents the molar mass of water, R the molar gas constant and the vapor pressure is described by an empiric approach according to Antoine.

$$\frac{dm_{(t)}}{dt} = \frac{k_M}{R}\left[\frac{p_{v\,(T_{dr},t)}}{T_{dr\,(t)}} - \frac{X_g * p_{v\,(T_g)}}{T_g}\right] * \\ * A_{sf\,(t)} * M_{H2O} * (-1) \quad (13)$$

B. Non-isothermal decomposition of urea

Once the droplets are injected into the exhaust gas stream, convective heat transfer from the surrounding gas to the droplets occurs and thus evaporation starts. A direct decomposition of urea from the aqueous urea solution only takes place in a very limited extent. More likely there is a separation of urea and water prior to the formation of ammonia which takes place in two reaction steps according to (1) and (2). The quantitative description of the thermolytic decomposition according to (1) is implemented in the model by the application of a mathematical power law, (14). This first order power law describes the correlation between the reaction rate r, the reaction rate constant $k_{therm(T)}$ and the reacting agent concentration c_{urea}.

$$r_{(k,c_{Urea})} = k_{therm\,(T)} * {c_{Urea}}^{n} \quad (14)$$

The temperature dependency of the reaction rate constant for thermolysis is calculated according to Arrhenius, (15) [7].

$$k_{therm} = 4{,}9 * 10^3 * \exp(-\frac{23066}{R * T}) \quad (15)$$

The self-adjusting temperature within the droplet is calculated by the balance of heat, which depends on the heat flux from the exhaust gas and the heat consumption due to the endothermic reaction, (16). The heat transfer coefficient is represented by k_w, the weight of the droplet by m_{dr} and the reaction enthalpy by H_{Therm}.

$$\frac{dQ}{dt} = k_w * A_{sf} * \left(T_g - T_{dr}\right) + \\ + \left(m_{dr\,0} - m_{dr\,(t)}\right) * (-H_{Therm}) \quad (16)$$

Rearranging and inserting the specific heat capacity of the droplet $c_{p\,dr}$ delivers the current droplet temperature, (17).

$$\frac{dT}{dt} = \frac{k_w * A_{sf} * \left(T_g - T_{dr}\right)}{m_{dr\,(t)} * c_{p\,dr\,(t)}} + \\ + \frac{\left(m_{dr\,0} - m_{dr\,(t)}\right) * (-H_{Therm})}{m_{dr\,(t)} * c_{p\,dr\,(t)}} \quad (17)$$

As a result, the simulation model is finally able to take weight losses due to evaporation and/or chemical reaction into consideration. Therefore, a more precise calculation of the droplets' motion can be performed. The final computation was carried out by a conventional numerical solver based on Euler.

C. Operation points and injection position

The temperature of the exhaust gas and its flow velocity strongly influences the trajectories of the droplets and depends on the current operation point (OP) of the diesel engine. To cover a broad range of operating conditions, the following operation points were chosen, Table 1:

Table 1: Exhaust gas mass flow and gas temperature of the investigated operation points

	mass flow (kg·h^{-1})	temperature (K)
OP 1	100	523
OP 2	350	723
OP 2	900	773

Initial spray parameters of the injection nozzle like the exit velocity, the cone angle or the size distribution were determined empirically by high speed recordings and laser diffraction.

The geometry of the mixing section is depicted in Fig. 4.

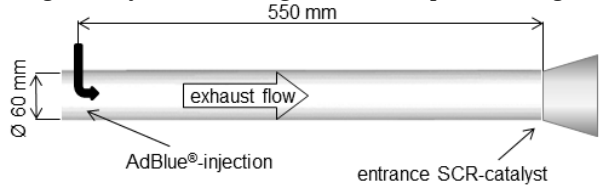

Fig. 4: Investigated mixing section

IV. Discussion of Results

A. Evaporation and thermal decomposition on a non-moving droplet

To enhance the knowledge of the chronological sequence of ammonia generation in SCR-systems the first simulations were performed for a non-moving, static droplet. To illustrate the difference in the behavior of UWS and water the calculations were performed for a pure water droplet as well.

The result of the simulations, depicted in Fig. 5, show a sharp temporal delimitation of the sub-steps during ammonia

formation. The graphs show the calculated profile of the droplets weight for a droplet of pure water, an UWS-droplet and the time-dependent mass fraction of urea in the UWS-droplet.

The reason for the faster weight loss of the water droplet can be found in the missing lowering of vapor pressure by dissolved urea. Additionally the progress of the droplet temperature is shown for the urea-water mixture. The evaporation of water out of an UWS droplet is described to be isothermal by Wozniak in [6].

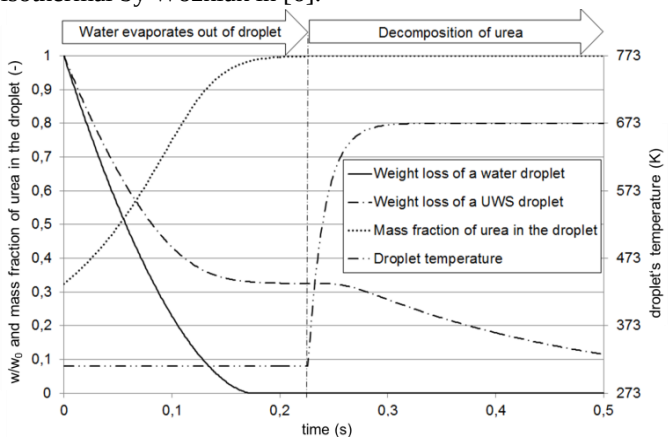

Fig. 5: Graphs of the droplet`s weight of pure water and UWS and the droplet temperature of UWS calculated at T_g = 600 K, initial droplet temperature T_{dr} = 303 K, u_{rel} = 0 m/s, D_{dr0} = 70 µm, k_0 = 4.9 * 103 1/s and $E_{A\ Therm}$ = 23066 J/mol [8]

The total amount of heat, which is transferred from the exhaust gas to the droplet, is used for evaporation and the temperature in the droplet remains at a steady state level. After the segregation-phase of water and urea in the droplet, recognizable by the mass fraction of urea achieving one, the droplet's temperature increases. With increasing temperature of the droplet the reaction rate constant of the thermolysis increases too and accelerates the reaction.

A second steady state level is reached as soon as a thermal equilibrium in the droplet between heat input by the exhaust gas and the applied heat of reaction is adjusted. This steady state temperature is very close to the ambient gas temperature. The reason for this can be found in the high heat transfer between exhaust gas and droplet and the moderate required heat for the reaction [8].

B. Model validation and plausibility check

To prove the validity of the simulation model, an experiment using laser diffraction was carried out. For this purpose the droplet size distribution in the mixing zone was determined 0.15 m downstream of the UWS-injection position. According to the model-based calculations a small part of the droplet spectrum must follow directly the exhaust gas flow and can be detected by laser diffraction. Droplets of larger diameter classes are undetectable. Because of its inertia they interpenetrate the exhaust gas flow, hit the opposite wall and deposit there, Fig. 6.

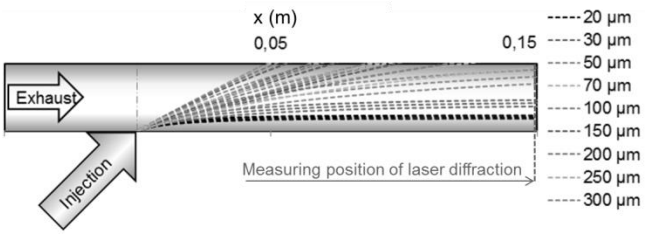

Fig. 6: Simulated droplet´s trajectories up to the measuring position of laser diffraction

Fig. 7 shows the comparison of the results of the simulation model and the experimental output. The experiment and the simulation results show that the droplets` size distribution decreases significantly 0.15 m downstream the UWS-injection, which is explainable by the wall contact and deposition of bigger size classes of the initial droplet spectrum.

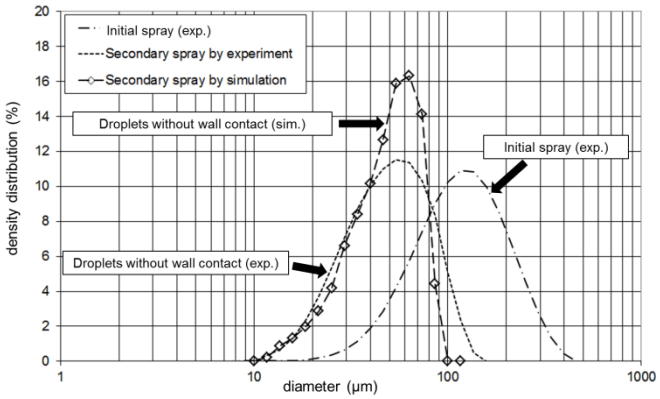

Fig. 7: Size distributions of the primary spray compared with the measured and calculated secondary spray after wall contact [8]

The comparison shows generally a good conformity of the diameter classes which are able to follow the exhaust gas flow between the model-based calculations and the experiment. Only the relative frequency at the relative maximum shows inaccuracies. The reason for this might be the method of analysis with discrete diameter classes and on the other hand deviations caused by the resolution of the laser diffraction measurement.

C. Trajectories of droplets

Fig. 8, Fig. 9 and Fig. 10 illustrate the trajectories of the droplets for the intended centered coflow and counterflow-injection.

The comparative consideration of the coflow- and counterflow-injection position shows that the droplets´ deflection by the exhaust gas after injection strongly depends on the operation point.

The summary for the conducted pre-studies is that only droplets smaller than 50 µm can follow the exhaust gas. Droplets of larger size classes will suffer wall contact before entering the catalytic converter and will not be content of the following discussion.

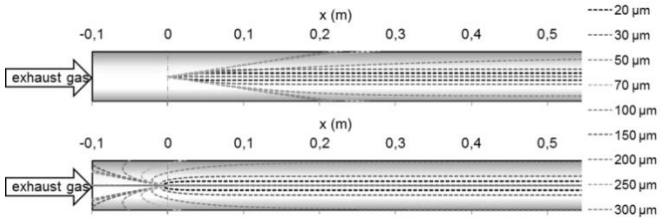

Fig. 8: Trajectories of droplets for coflow- and counterflow-injection in OP1

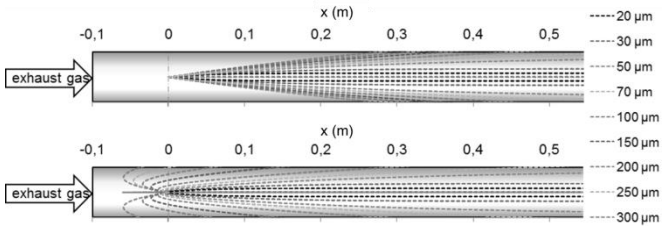

Fig. 9: Trajectories of droplets for coflow- and counterflow-injection in OP2

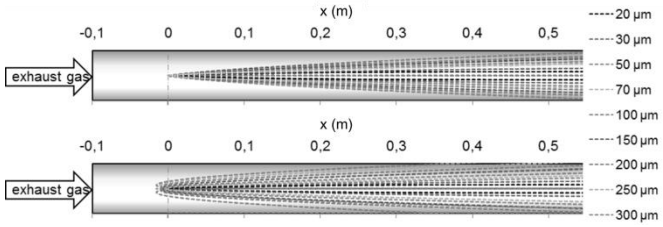

Fig. 10: Trajectories of droplets for coflow- and counterflow-injection in OP3

D. Weight losses on droplets

The ideal case would be a complete evaporation of water out of the UWS-droplet and a consecutively complete thermolysis. Fig. 11 shows comparatively the weight losses of droplets with an initial diameter of 50 µm for different injection directions in relation to the residence time inside the mixing section. The resulting residence times of the droplets before entering the catalytic converter differ due to the injection variants and the differences in the travelled path lengths of the droplets. The x-marks in the figure represent the moment of entering the catalytic converter.

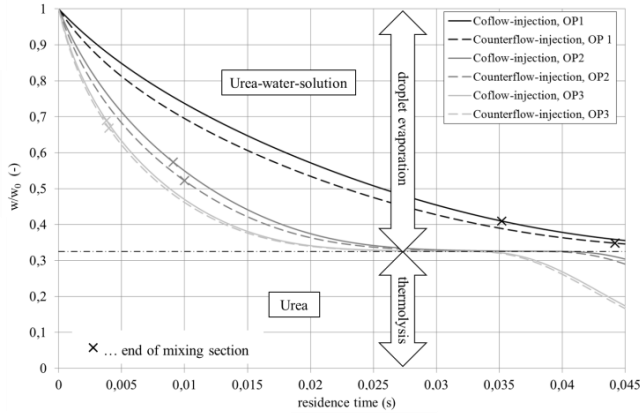

Fig. 11: Loss of droplet`s weight for the investigated injection geometries during the flight phase in the mixing section

Furthermore Fig. 11 shows that droplets which are inserted in counterflow direction experience a longer residence time in the mixing section and the evaporation endures longer which results in higher weight losses. In principle this effect is detectable for all operation points, but the biggest occurrence inside the mixing section can be determined at low-load operation points, e.g. OP1.

For none of the investigated injection geometries and operation points could be confirmed that evaporation and thermolysis are completed inside the mixing section. The segregation of UWS and the evaporation of water were completed by achieving a mass fraction of 0.325 that is equal to the initial mass fraction of urea in the UWS. This implicates that liquid droplets enter the catalytic converter, occupy active centers on the catalyst and reduce the entire efficiency of the SCR-system.

Another factor for differences in the weight loss is that the relative velocity between the droplet and the surrounding exhaust gas depends on the injection geometry. The highest relative velocities and further the highest weight losses can be expected for counterflow-injections. This is reasoned by higher Reynolds numbers, according to (18) and (5).

$$\vec{u}_{rel} = \vec{u}_g - \vec{u}_{dr} \tag{18}$$

High Reynolds numbers are responsible for increasing heat and mass transfer coefficients k_w and k_m, shown in (10) and (16). The progresses of the Reynolds numbers for the investigated 50 µm droplets are illustrated in Fig. 12. It depicts that the Reynolds number decreases with longer residence times in the mixing section due to the fact that the velocity of the droplet converges to the velocity of the exhaust gas flow. The Reynolds number is directly influenced by the relative velocity u_{rel} and the droplet´s diameter, (15). The highest Reynolds numbers occur just after the injection and are furthermore considerably higher for counterflow injections.

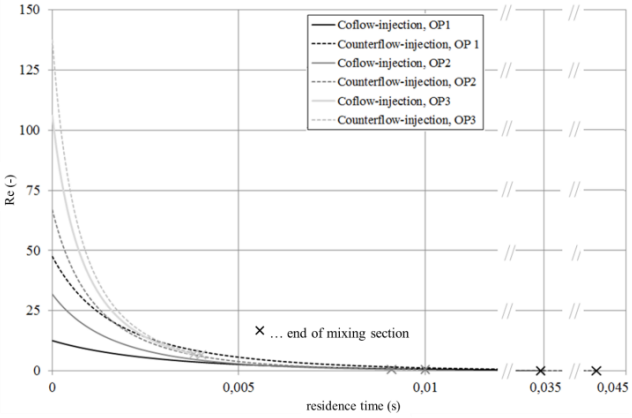

Fig. 12: Progress of the Reynolds number during the flight phase of a 50 µm droplet in the mixing section

Fig. 13 describes the progress of the relative velocity u_{rel} and the diameter of the droplet with an initial diameter of 50 µm during the flight phase in the mixing section. As expected, the highest relative velocities can be detected for the counterflow-injections at OP3.

The comparison of the initial relative velocities illustrates that the counterflow-injection is higher by more than one order of magnitude. In contrast to the initial values, the further

progresses of the relative velocities show equalization after approximately 0.01 s. The comparison of the graphs shows that the decreasing diameter of the droplet plays a minor role for influencing the Reynolds number, the main effect is caused by changes in the relative velocity u_{rel}.

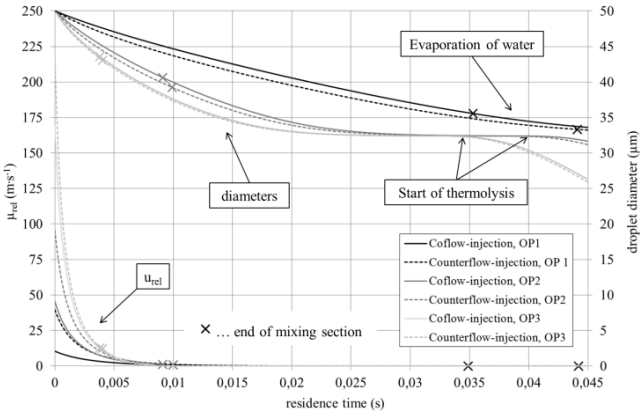

Fig. 13: Course of the relative velocity between droplet and exhaust gas and the droplet diameter in the mixing section

The progresses of the heat transfer and the mass transfer coefficients are illustrated in Fig. 14 and Fig. 15 and show a qualitative similarity.

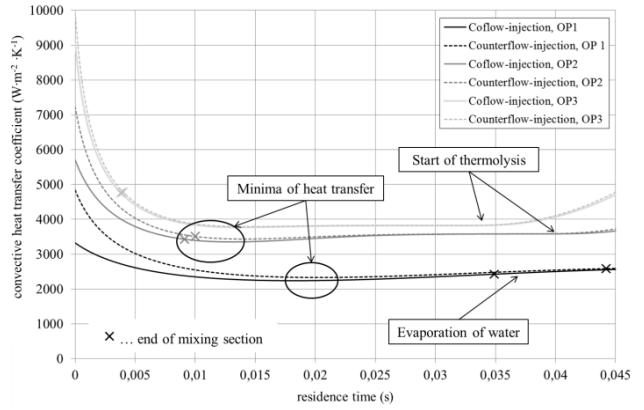

Fig. 14: Progress of the convective heat transfer coefficient during the flight phase of a 50 µm droplet in the mixing section

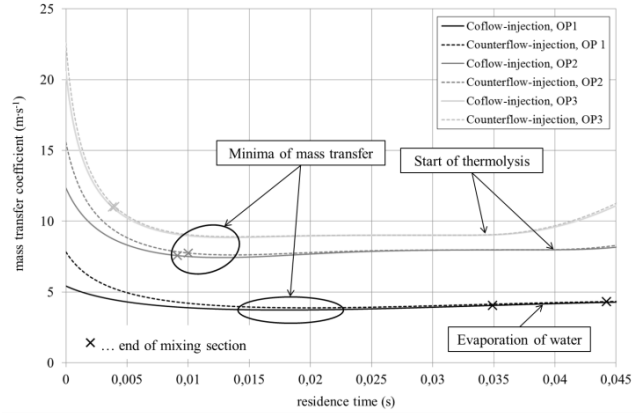

Fig. 15: Progress of the mass transfer coefficient during the flight phase of a 50 µm droplet in the mixing section

In particular the graphs of coflow- and counterflow-injection show a specific course. Both values start at maxima due to high Reynold numbers caused by high relative velocities. During the flight phase of the droplet in the exhaust gas the relative velocity converges to the exhaust gas velocity and the Reynolds number moves towards zero and decreases the heat and mass transfer until temporary minima. After passing the minima the transfer coefficients start increasing slightly. The reason for this particular behavior will be discussed after the implementation of the Nusselt number and the calculation of the heat transfer coefficient by (19).

The heat transfer coefficient depends on the Reynolds number, the characteristic length (= droplet diameter), the heat conductivity of the surrounding exhaust gas λ_g and the Prandtl number Pr. The determination of the Prandtl number is shown in (20) and is influenced by the dynamic viscosity μ_g and the heat capacity $c_{p\,g}$ of the exhaust gas.

$$Nu_{(t)} \equiv \frac{k_w * D_{dr(t)}}{\lambda_g} = \\ = 2 + 0{,}6 * Re_{dr(t)}^{\frac{1}{2}} * Pr^{\frac{1}{3}} \tag{19}$$

$$Pr = \frac{\mu_g * c_{p\,g}}{\lambda_g} \tag{20}$$

The comparison of the quantitative heat and mass transfer on droplets can be done by simplifying and rearranging (10) and (19). Through reducing the primary equations by all constants they finally show a similar structure, (21) and explain the course of the graphs in Fig. 14 and Fig. 15. The letter z represents in this equation either the heat conductivity of the exhaust gas λ_g for the heat transfer or the diffusion coefficient of vapour into air for the mass transfer.

$$k_{(u_{rel},\,D_{dr})} = \frac{2 * z + f_{(u_{rel},\,D_{dr})}}{D_{dr}} \tag{21}$$

The character "2" in (10), (19) and (21) stands for the lower limiting value for the transfer coefficients on spheres like ideal droplets. The derivation takes places by introducing the minimal heat transfer coefficient $\breve{\alpha}$, which takes place for the case $Re_{dr\,L'} \rightarrow 0$. Furthermore it includes the heat conductivity λ_g and the radius r, (22).

$$\breve{\alpha} = \frac{\lambda_g}{r} \tag{22}$$

For spherical bodies (23) is taken into account by inserting the overflowed length L´, which is the ratio of the surface area and the projected circumference.

$$Nu = \breve{\alpha} * \frac{L'}{\lambda_g} \tag{23}$$

Inserting the droplet diameter for L´ and L´/2 for r delivers finally (24) [9].

$$\breve{N}u_{L'} = 2 \tag{24}$$

The Nusselt number for a static surrounding gas atmosphere $\breve{N}u_{L'} = 2$ can be inserted into (19) and results in the solution for the minimum value of the heat transfer coefficient, (25).

$$k_{w\,min} = \frac{2 * \lambda_g}{D_{dr}} \tag{25}$$

In analogy to (25) the minimum of the mass transfer coefficient can be set by inserting (24) in (10) where the Sherwood number replaces the Nusselt number, (26).

$$k_{m\,min} = \frac{2 * D}{D_{dr}} \tag{26}$$

In both cases, the heat transfer and the mass transfer, it can be stated that the transfer coefficients do not underrun a minimum. For $Re_{dr'} \rightarrow 0$ the convective heat transfer is transformed into heat conduction and the mass transport is converted into a diffusion phenomenon. Fig. 16 shows and explains the regimes of heat and mass transfer on a drop with different relative velocities and differing Reynolds numbers.

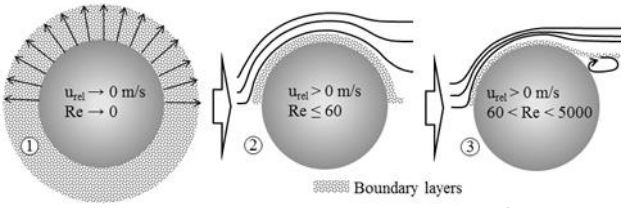

Fig. 16: Non-moving droplet in a static atmosphere ①, a moderate moving droplet with attached flow profile ② and a rapidly moving droplet with separation of laminar flow and turbulences ③.

V. Conclusion

In the course of this study a numerical model was established, which is able to describe the trajectories of droplets in an exhaust gas flow of an SCR-system. In contrast, to previous studies the model is able to describe the segregation of UWS caused by droplet evaporation and consequently thermal decomposition of pure urea. Furthermore, the sharp limitation between evaporation and thermal decomposition could be confirmed by previous experiments.

The validity of the model could be proved by experiments using laser diffraction which confirms the explanatory power of the simulation model.

It could be shown that an exemplary droplet of 50 µm will not evaporate completely inside the mixing section independently from the injection direction. The fact that the evaporation of water and the thermolysis will occur partly in the catalytic converter reduces the overall efficiency of SCR-systems.

The particular comparison between coflow- and counterflow-injection shows advantages for the counterflow-injection due to longer residence times in the mixing section and higher relative velocities which result in higher heat and mass transfer coefficients. The highest weight losses can be achieved by long residence times whereas the influence of the exhaust gas temperature and relative velocity is secondary. The reason for this is that the droplets´ velocity converges very fast with the exhaust gas velocity which results in strongly decreasing Reynolds numbers during the droplets´ flight phase.

The progress of the heat and mass transfer coefficients on the free moving droplet show a slight rise after temporary minima, which is caused by lower limiting transfer coefficients. The existence of this minimal transfer coefficient for spherical bodies could be confirmed by derivation of Prandtl´s theory of boundary layers.

The heat and mass transfer during the flight phase effects only droplets of comparably small diameter classes because bigger droplets can interpenetrate the exhaust gas flow due to their higher kinetic energy. These bigger droplet size classes which cannot follow the exhaust gas flow suffer wall contact and experience another path of evaporation and thermal decomposition.

References

[1] M. Weißbäck, *Erfüllung zukünftiger Emissionsanforderungen für Diesel SUV`s*. Forschungsgesellschaft Kraftfahrwesen mbH Aachen, 15. Aachener Kolloquium Fahrzeug- und Motorentechnik, Tagungsband Nr. 1506, 2006.

[2] G. Merker, *Verbrennungsmotoren*. Wiesbaden: B. G. Teubner, ISBN-10 3-8351-0080-7, 2006.

[3] S. Fischer, *Simulation of the Urea-Water-Solution Preparation and Ammonia-Homogenization with a Validated CFD-Model*. Dissertation at Vienna University of Technology, 2012.

[4] F. Birkhold, *Selektive katalytische Reduktion von Stickoxiden in Kraftfahrzeugen: Untersuchung der Einspritzung von Harnstoff-Wasserlösung*. Dissertation an der Universität Stuttgart, 2007.

[5] W. Ranz, W. Marshall, *Evaporation from drops.* Chem. Eng. Prog., Vol. 48, 1952.

[6] G. Wozniak, *Zerstäubungstechnik*. ISBN 3-540-41170-4: Springer, 2003.

[7] S. Yim, *Decomposition of Urea into NH3 for the SCR-Process*. Industrial & Engineering Chemistry Research: American Chemical Society, Volume 43, Page 4856-4863, 2004.

[8] L. Möltner, *Tropfen/Abgas- und Tropfen/Wandinteraktionen von AdBlue bei der selektiven katalytischen Reduktion von Stickoxiden*. Fortschritt-Berichte VDI Reihe 12 Verkehrstechnik/Fahrzeugtechnik Nr. 785, VDI Verlag Düsseldorf, ISBN 978-3-18-378512-4, 2014.

[9] W. Wagner, *Wärmeübertragung*. Vogel-Buchverlag, 6. Auflage, ISBN 978-3-8023-1974-5, 2004.